JOURNAL OF CHEMICAL INFORMATION AND MODELING

LETTER

pubs.acs.org/jcim

Aggregation Properties of a Polymeric Anticancer Therapeutic: A Coarse-Grained Modeling Study

Lili X. Peng,[†] Lei Yu,[§] Stephen B. Howell,[‡] and David A. Gough*,[†]

[†]Department of Bioengineering, [‡]Moores Cancer Center, University of California, San Diego, La Jolla, California

[§]Nitto Denko Technical Corporation, Oceanside, California

Supporting Information

ABSTRACT:

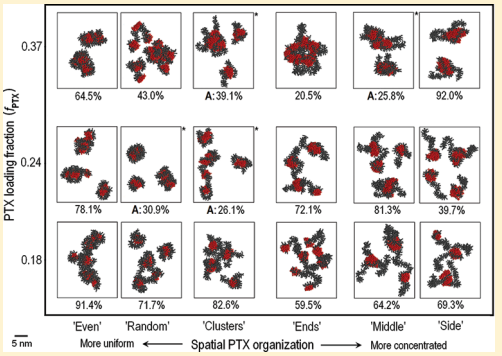

The effects of paclitaxel (PTX) loading fraction and spatial PTX arrangement on poly(γ-glutamyl-glutamate) paclitaxel (PGG-PTX) aggregation were explored using coarse-grained molecular dynamics. Results show that the PTX loading fraction does not significantly impact aggregation, and the spatial PTX arrangement only affects aggregation at more concentrated PTX arrangements. Overall, the f_{PTX} = 0.37 'ends' and f_{PTX} = 0.18 'even' PGG-PTX systems exhibit the highest aggregation and the 'middle' and 'side' systems the lowest.

An ongoing challenge in the development of efficacious anticancer therapeutics is ensuring that sufficient amounts of the administered biologic reach the diseased target while simultaneously limiting its cytotoxic exposure to healthy tissues and cells.[1,2] The enhanced permeability and retention effect has served as a key rationale for the transport of a therapeutic agent from systemic circulation to tumor cells. The therapeutic nanoparticle must first flow to tumors via blood vessels, diffuse through fenestrations of the leaky tumor vasculature, and finally penetrate through interstitial space to reach the target cells.[2−5] Although the precise cause-effect relationship of nanoparticle toxicity is not very well understood, studies have suggested that the ability of nanoparticles in crossing these barriers is significantly influenced by their fundamental properties, such as size, shape, surface charge, and aggregation propensity.[6,7] There is increasing concern that nanoparticles smaller than cells of normal tissue are capable of penetrating these biological structures and disrupting normal cell function.[8] However, in an aggregate state, nanoparticles are larger and, depending on the size of the aggregate, may not be able to bypass natural cellular barriers, potentially reducing toxicity. Moos et al. demonstrated that 40 nm zinc oxide spheres exhibit more potent toxicity than their 330 nm spherical counterparts.[9] Similarly, experimental work by Pan et al. on colloidal gold nanoparticles has shown that particles 1−2 nm in size are highly toxic, while the 15 nm gold colloids are relatively nontoxic; this behavior was consistent across four different *in vitro* cell lines.[10] These implications suggest the aggregation propensity of therapeutic nanoparticles as the foundation for their clinical design.

This study uses computational modeling to explore how the aggregation of poly(γ-glutamyl-glutamate) paclitaxel (PGG-PTX), a polymer-drug conjugate in preclinical development as an anticancer therapeutic, is affected by PTX loading fraction (f_{PTX}) and PTX location on the 130-mer PGG backbone. Molecular simulations can provide useful insight on the physicochemical properties of PGG-PTX, which can otherwise be difficult to acquire experimentally.[11] The results can be used to direct experimental testing on candidate formulations using *in vitro* and *in vivo* models in preclinical trials, an arduous and tedious process that can take up to on average five to seven years.[12] Therefore, insight on the aggregation propensity of PGG-PTX can be used to facilitate its preclinical development. At the commencement of this study, the only PGG-PTX formulations under serious consideration for clinical translation varied in f_{PTX} of 0.18 ($MW_{PGG\text{-}PTX} \sim 43\,900$ Da), 0.24 ($MW_{PGG\text{-}PTX} \sim 49\,700$ Da), and 0.37 ($MW_{PGG\text{-}PTX} \sim 56\,200$ Da), which correspond to 12, 19, and 26 paclitaxels on an 130-mer PGG backbone, respectively.[13] Since the chemical formulations for PGG-PTX had already been decided prior to this work, we only focused on predicting aggregation the PGG-PTX formulations being considered as potential chemotherapeutics. Therefore, molecular models of PGG-PTX were created such that PTX molecules were conjugated onto the PGG backbone in six patterns ('even', 'random', 'clusters', 'ends', 'middle', and 'side') for each PTX loading fraction, resulting in a library of 18 PGG-PTX molecules (see Figure S1, Supporting Information).

To date, computational methodologies for predicting protein aggregation that have obtained respectable experimental validation involve predicting fibrillar and β-sheet formation and locating hydrophobic "hot spots" for aggregation based on amino acid sequence.[14−22] Methodologies have been developed for both atomistic and coarse-grained (CG) models. We have considered using these bottom-up approaches to predict PGG-PTX aggregation propensity, but application of these methods to PGG-PTX is not suitable due to fundamental differences in shape and chemical composition of PGG-PTX and proteins.

Published: October 13, 2011

Regarding shape, PGG-PTX has been shown by circular dichroism spectroscopy to exist as a random coil and thus will most likely not form fibrils or adopt any secondary structure. Regarding chemical composition, PGG-PTX is comprised of glutamyl-glutamate and glutamyl-glutamate paclitaxel monomers, not amino acids. To have the utility to predict PGG-PTX aggregation using a bottom-up approach based on random coil morphology and organic monomer composition would be ideal, but a thorough literature review only revealed an absence of such a method. We then considered designing our own bottom-up method of developing a hydrophobicity scale for glutamyl-glutamate and glutamyl-glutamate paclitaxel residues, similar to the hydrophobicity scales for amino acids based on their physical properties, such as surface tension, molar heat capacity, and transition temperature. However, such a task would require a tremendous amount of work that would exceed the confines of this study, not to mention the majority of the bottom-up methods for protein aggregation are tailored toward predicting aggregation of a single protein. Our primary focus was to identify the most promising therapeutic candidates out of 18 different PGG-PTX variants based on their propensities to aggregate. Given these circumstances, we were left to devise a more efficient aggregation prediction methodology for PGG-PTX.

Prior to conception of a new method, the fundamental physicochemical behavior represented by "aggregation" must be elucidated. A literature review revealed that definition of "aggregation" varies widely depending on the source, ranging from "an assemblage of particles loosely attached by contact at the corners and edges" to "an assemblage of particles rigidly and firmly bound at their faces by fusion, sintering, or growth". To make matters more confusing, the term "aggregation" is often used indiscriminately from its cousin term, "agglomeration".[23] Therefore, for simplicity and to allay confusion, we decided on the former definition of an aggregate: an assemblage of particles loosely held together by contact at the corners and edges. Once this definition had been established, we then analyzed the aggregation propensity of PGG-PTX systems based on the intermolecular distance among individual PGG-PTX molecules. While our distance-based approach is inherently different from the aforementioned bottom-up methodologies for predicting protein aggregation, our goal was to obtain a general idea of the aggregation propensity for a virtual library of potential anticancer polymer-drug variants in an expedient and high-throughput manner.

Before simulating PGG-PTX aggregation, the initial structure must be decided. Our previous circular dichroism spectroscopy studies indicated that PGG-PTX exists as a flexible random coil, suggesting that molecular dynamics (MD) simulations of PGG-PTX can be commenced from any structure. Furthermore, to address the issue of simulation time, consideration was given to the random coil nature of PGG-PTX: since PGG-PTX is a random coil, it most likely exists as a range of structurally similar conformations rather than as a static conformation.[24] Thus, we ran MD simulations until minimal movement of PGG-PTX persisted at the molecular level, or a statistical equilibrium, at which each PGG-PTX system exists as a dynamic ensemble of statistically related conformations (see Figure S2, Supporting Information).

CG models of each of the 18 PGG-PTX molecules have been developed using the MARrink Toolkit INItiative (MARTINI) force field, which has been shown to have excellent experimental reproducibility for amino acids.[25−27] Validation of each of the 18 CG PGG-PTX models had been done by comparing the equilibrium bonded parameters from the CG models with those determined from simulations of atomistic PGG-PTX models. The results demonstrated that the equilibrium bonded parameters of the CG PGG-PTX models successfully reproduced the equilibrium bonded parameters of the AA PGG-PTX models.[24]

To mimic the initial vial concentration of 50 mg/mL, five PGG-PTX molecules were placed in cubic box sizes of (19.4 × 19.4 × 19.4 nm), (20.2 × 20.2 × 20.2 nm), and (21.2 × 21.2 × 21.2 nm) for the f_{PTX} = 0.18, 0.24, and 0.37 systems, respectively (refer to Scheme S1, Supporting Information, for exact calculation).[13] Periodic boundary conditions (PBC), a conventional method used to study bulk properties of a biomolecular system by modeling a small portion far from its edge, were applied to each simulation box. (PBC imposes that the simulation box is replicated in all three Cartesian coordinates to form an infinite lattice.[28]) To ensure system neutrality, the negative charges of -1240, -1205, and -1170 imparted by the glutamyl-glutamate residues of the f_{PTX} = 0.18, 0.24, and 0.37 systems, respectively, required the replacement of 1240, 1205, and 1170 CG water beads with sodium ions for the three respective systems. (Detailed calculations are provided in Scheme S1.) We were aware that adding counterions to the PGG-PTX system may undesirably influence bias the resulting behavior of PGG-PTX molecules. Therefore, to determine the sensitivity of the CG PGG-PTX systems to charge state, we ran 2 μs MD simulations of eight randomly selected PGG-PTX systems in pure explicit water without counterions and then compared the resulting physicochemical properties (radius of gyration, root-mean-squared fluctuation, and aggregation number) with those of the original CG PGG-PTX systems neutralized with Na+ ions for the first 2 μs (effective time) of the MD trajectories. (Figures S2−S4, Supporting Information, demonstrate that the addition of the aforementioned numbers of Na+ ions to the eight PGG-PTX systems does not significantly impact the size, flexibility, and aggregation propensity of PGG-PTX molecules.)

The governing mathematical equations for the CG MD, mapping of atomistic models to CG models, and CG parametrization of PGG-PTX molecules have been described.[24] The NPT ensemble (the number of particles N, pressure P, and temperature T were all fixed) was applied for the simulations; the temperature was kept at 310 K with a coupling constant of τ_T = 0.1 ps; and the pressure was weakly coupled to 1 bar with a relaxation time of τ_P = 0.5 ps. The cutoff length for the nonbonded interactions was r_{cut} = 1.2 nm. Lennard-Jones and Coulombic forces were considered for r_{cut} < 0.9 nm and r_{cut} < 1.2 nm, respectively, and Coulombic forces were computed every time step for 1.0 nm and once every 10 time steps for 0.9 nm < r_{cut} < 1.2 nm. The time step in the leapfrog integration scheme was 5 fs. The energies, coordinates, and velocities were written every 0.5 ps. MD simulations were run until a statistical equilibrium was reached at 3 μs. The time scale was scaled up by a factor of 4 because CG dynamics is faster than atomistic dynamics, due to the smoothness of the CG interactions. This factor of 4 is based on the speedup in the diffusional dynamics of CG water as compared to AA water. Therefore, the simulation time scale was scaled up by a factor of 4 resulting in an effective time of 12 μs.[26,27]

The structural conformations of the 18 PGG-PTX systems were analyzed using root-mean-squared deviation (RMSD) clustering, a quantitative method that categorizes all conformations accessed during the MD trajectory into clusters based on structural similarity.[24,29] For each PGG-PTX system, the RMSD

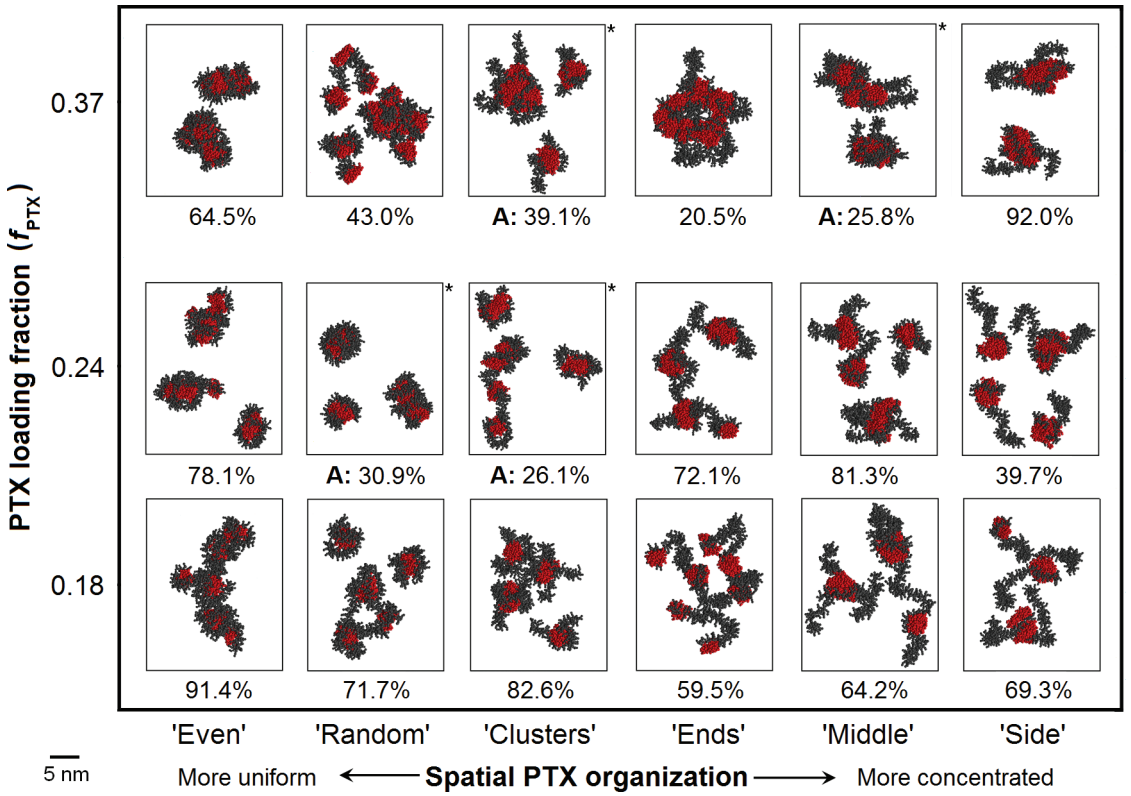

Figure 1. Predominant unique, significant characteristic conformations of all PGG-PTX systems as a function of PTX loading fraction and spatial PTX arrangement. Shows the paclitaxel (*red*) and glutamyl-glutamate (*gray*) residues of each PGG-PTX molecule. The percentage below each box indicates the population of frames corresponding to the each unique, significant characteristic conformation for the 12 μs MD trajectory or the percentage trajectory occupancy. For systems with more than one unique, significant characteristic conformation, their most significant, unique characteristic conformation is denoted with an asterisk (*), and less significant, unique characteristic conformation(s) is shown in Figure S3.

cutoff was optimized in the GROMACS 4.0.3 *g_cluster* module to meet the following criteria: (1) the total number of clusters was approximately 40; (2) 90% of the trajectory was contained in clusters fewer than 40; and (3) very few clusters included one configuration (see Table S1, Supporting Information). Those PGG-PTX systems possessing multiple characteristic conformations were then assessed for uniqueness based on the following criterion using the RMSD calculator tool in Visual Molecular Dynamics 1.8.6:[30] if the RMSD between each significant characteristic conformation were greater than twice the RMSD cutoff, then the significant conformation(s) was/were deemed unique (see Table S1). Since each PGG-PTX system could possess up to ~40 unique characteristic conformations, only those statistically significant, or occupying at least 10% of the 12 μs trajectory, were respected. (A detailed, step-by-step procedure for determining significance and uniqueness of a sample PGG-PTX system, f_{PTX} = 0.18 'ends', is shown in Scheme S2, Supporting Information.) Finally, a PDB structure was extracted from each unique, significant characteristic conformation.

Figure 1 shows the predominant unique, significant characteristic conformations of the 18 PGG-PTX aggregates as a function of PTX loading fraction and spatial PTX arrangement. (For PGG-PTX systems with multiple unique, significant characteristic conformations, the less significant conformations are shown in Figure S5, Supporting Information.) It is apparent that PGG-PTX molecules with more uniform PTX arrangements ('even' and 'random') are characterized by spherical, globular shapes, whereas systems with more concentrated PTX arrangements ('middle' and 'side') have filamentous, wormlike shapes. PGG-PTX molecules with clustered PTX arrangements ('clustered' and 'ends') exhibit both spherical and filamentous behavior, as evidenced by the partially spherical f_{PTX} = 0.24 'clusters' molecules and filamentous f_{PTX} = 0.18 'ends' molecules. This behavior is consistent at f_{PTX} = 0.18 and 0.24; at f_{PTX} = 0.37, however, the shape of each individual PGG-PTX molecule becomes less distinguishable, most likely due to increasing interactions among neighboring PGG-PTX molecules.

The aggregation behavior of each PGG-PTX system was assessed by the number of CG beads with respect to the distance from the system's center-of-gravity (COG), d_{COG}, and the minimum intermolecular distance among the five PGG-PTX molecules within a system, d_{min}. A higher CG bead number suggests a higher propensity for aggregation at a certain d_{COG}. In Figure S6, Supporting Information, the f_{PTX} = 0.37 systems have the highest number of CG beads overall; the f_{PTX} = 0.18 systems the lowest. This behavior is expected since the $MW_{PGG\text{-}PTX}$ is the highest and lowest for the f_{PTX} = 0.37 and 0.18 molecules, respectively. Therefore, to assess the aggregation of PGG-PTX system independent of its molecular weight, the ratio of CG beads (at a particular d_{COG}) to the total number of CG beads comprising each PGG-PTX system was determined with respect to the d_{COG} of each PGG-PTX system and displayed in Figure 2. In addition, PGG-PTX aggregation was analyzed from the d_{min} values among the five PGG-PTX molecules per system. For each PGG-PTX system, the minimum intermolecular distance between two out of five PGG-PTX molecules throughout the 12 μs MD

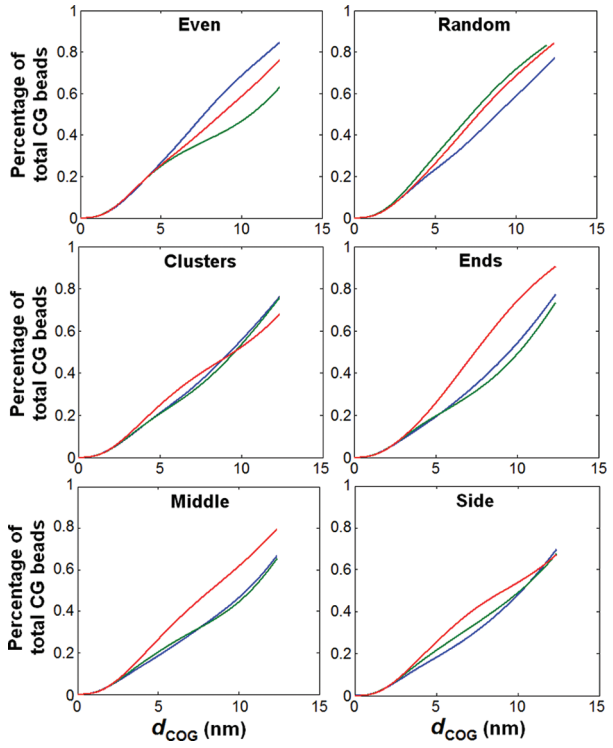

Figure 2. Percentage of CG beads of PGG-PTX systems from their respective COG. Data correspond to f_{PTX} = 0.18 (*blue*), 0.24 (*green*), and 0.37 (*red*) PGG-PTX systems. Values are based off of the total number of CG beads.

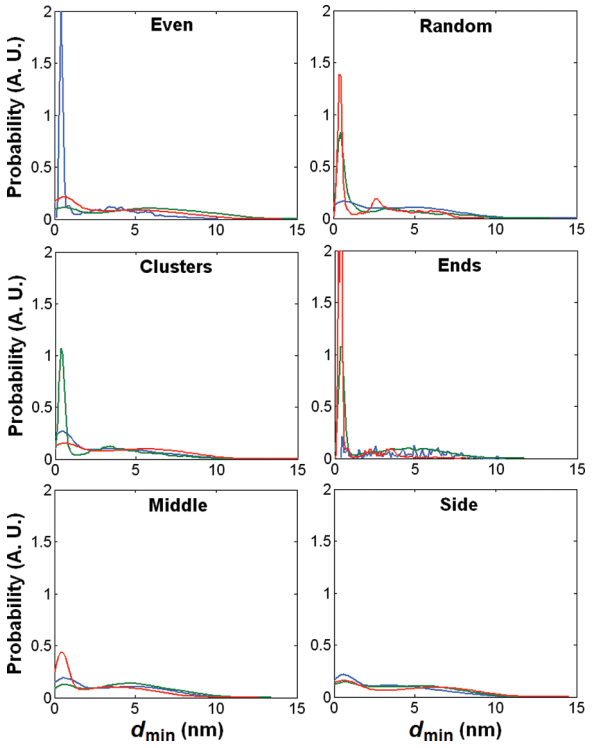

Figure 3. Probability distributions for minimum intermolecular distance among PGG-PTX molecules. Data correspond to f_{PTX} = 0.18 (*blue*), 0.24 (*green*), and 0.37 (*red*) PGG-PTX systems.

trajectory was extracted using the *g_mindist* module of GROMACS 4.0.3. A histogram of the d_{min} values was then taken and converted to a probability distribution using the *ksdensity* function in MATLAB 7.0.[32] Figure 3 shows the probability distributions for the d_{min} values for all PGG-PTX systems. The shape of the distribution signifies the degree of aggregation: a wider distribution with a flatter peak indicates that the PGG-PTX molecules are farther apart and lower aggregation, whereas a narrower distribution with a sharper peak suggests closer proximity among molecules and higher aggregation. Moreover, the d_{min} corresponding to the peak of the probability distribution indicates the proximity between PGG-PTX molecules for a particular system: a lower d_{min} near the peak indicates closer proximity and a higher degree of aggregation, whereas a lower degree of aggregation is characterized by a higher d_{min} near the peak.

Figure 2 proposes that the f_{PTX} = 0.37 'even' system has the highest degree of aggregation, as evidenced by the highest % CG bead number values that reach ∼90% at a d_{COG} ∼ 12 nm. This finding is further substantiated by the system's unique, significant characteristic conformations in Figure 2 and Figure S5, which indicate the presence of close and dense spatial packing of the five PGG-PTX molecules. Furthermore, Figure 3 shows that f_{PTX} = 0.37 'even' has the highest peak in its probability distribution curve at d_{min} ∼ 0.5 nm, suggesting that most of the PGG-PTX molecules are closely packed together during the majority of the 12 μs trajectory, another sign of high degree of aggregation.

Generally speaking, other PGG-PTX systems that exhibit a relatively strong tendency to aggregate include the f_{PTX} = 0.18 'even', f_{PTX} = 0.24 'random', and f_{PTX} = 0.37 'random', and f_{PTX} = 0.37 'middle'. Their % CG bead number values reach ∼80% by d_{COG} ∼ 12 nm, which is considerably high relative to those of other PGG-PTX systems. Also, their peaks in probability distribution curves in Figure 3 at low d_{min} values (∼0.5−1 nm) also signify tight spatial clustering of PGG-PTX molecules and relatively high aggregation. While similar behavior is prevalent in the f_{PTX} = 0.18 'even', f_{PTX} = 0.24 'random', and f_{PTX} = 0.37 'random', and f_{PTX} = 0.37 'middle' systems in Figures 2 and 3, slight differences in spatial conformation are actually witnessed in Figure 1 and Figure S5. For the f_{PTX} = 0.18 'even' system, it appears that the five PGG-PTX molecules tend to cohesively arrange themselves into a larger aggregate, whereas in the f_{PTX} = 0.24 'random', f_{PTX} = 0.37 'random', and f_{PTX} = 0.37 'middle' systems, intermolecular PGG-PTX interactions result in 2−3 smaller aggregates each comprised of 2−3 PGG-PTX molecules. Closer inspection of Figure 3 shows that the probability distribution values for the f_{PTX} = 0.24 'random', f_{PTX} = 0.37 'random', and f_{PTX} = 0.37 'middle' systems are distributed over a wider range of d_{min} values than that of the f_{PTX} = 0.18 'even' system. Moreover, the peaks in the probability distribution for the f_{PTX} = 0.24 'random', and f_{PTX} = 0.37 'random', and f_{PTX} = 0.37 'middle' systems are considerably lower than the peak of the f_{PTX} = 0.18 'even' system. Overall, the f_{PTX} = 0.18 'even' system tends to aggregate slightly more than the other three systems.

PGG-PTX systems exhibiting lower degrees of aggregation are the 'side' ones at all three PTX loading fractions, the 'middle' systems at f_{PTX} = 0.18 and 0.24, and the 'even' system at f_{PTX} = 0.24, as evidenced by the consistently low % CG bead values reaching only 60% by d_{COG} ∼ 12 nm. Their low aggregation behavior is further supported by the lack of a sharp peak in their respective probability distribution curves and the large range of

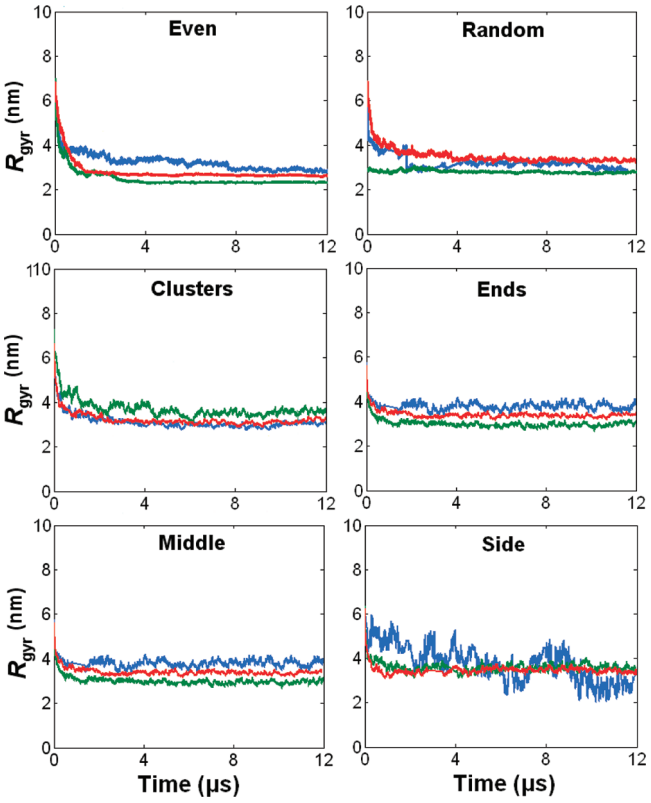

Figure 4. Average radius of gyration trajectories of individual PGG-PTX molecules per aggregate. Trajectories correspond to f_{PTX} = 0.18 (*blue*), 0.24 (*green*), and 0.37 (*red*) PGG-PTX systems.

d_{min} values accessed throughout the 12 μs MD trajectory. Figure 1 also shows that the PGG-PTX molecules tend to exist as individual entities, thus confirming the relatively low-aggregation behavior.

While a range of aggregation is witnessed in the 18 PGG-PTX systems, the size of the individual PGG-PTX molecules per system remains relatively constant across all PTX loading fractions and spatial PTX arrangements. Figure 4 shows the average radius of gyration (R_{gyr}) values for PGG-PTX molecules. Most molecules start out at $R_{gyr} \sim 6-8$ nm, decrease to $R_{gyr} \sim 3-4$ nm by 1 μs, and maintain that size until 12 μs. This data suggests that while the PTX loading fraction and spatial PTX arrangement impact the bulk aggregation, the size of each PGG-PTX molecule remains the same.

On the whole, our results suggest that, for PGG-PTX systems with more concentrated spatial PTX arrangements ('even', 'random', and 'clusters'), there is no apparent correlation between PTX loading fraction and PGG-PTX aggregation or between spatial PTX arrangement and PGG-PTX aggregation. However, PGG-PTX systems with more concentrated PTX arrangements ('middle' and 'side') tend to limit PGG-PTX aggregation at nearly all PTX loading fractions.

At the commencement of this study, we were curious to determine whether the PTX loading fraction and/or the spatial PTX arrangement offered any efficacious advantages in terms of controlling PGG-PTX aggregation. Our goal was to acquire useful theoretical information that may aid in the preclinical design and development of PGG-PTX and potentially improve its therapeutic efficacy in terms of reducing toxic effects to normal tissue. MD simulations on 18 PGG-PTX models, each with a unique combination of PTX loading fraction (0.18, 0.24, and 0.37) and spatial PTX arrangement ('even', 'random', 'clusters', 'ends', 'middle', and 'side'), were run for 12 μs. In general, the 'middle' and 'side' PGG-PTX systems exhibit the lowest aggregation, suggesting that they are most likely to bypass cellular barriers, thus promoting higher toxicity. On the contrary, the f_{PTX} = 0.37 'ends' and f_{PTX} = 0.18 'even' systems are the most likely to minimize toxicity, as their higher aggregation state suggests a lower propensity for cell permeation. In conclusion, the f_{PTX} = 0.37 'ends' and f_{PTX} = 0.18 'even' PGG-PTX systems are the most therapeutically promising candidates and are recommended for further experimental testing.

In closing, our distance-based methodology presented here is by no means fully complete. Experimental validation of the aggregation results is still necessary to refine and improve the methodology. Our previous MD work on unimolecular PGG-PTX molecules allowed for the ease of implementation of MD simulations of multiple PGG-PTX molecules for assessing aggregation. However, toward the end of this study we were alerted to other, although somewhat obscure, distance-based approaches that had been developed for polymer systems. Cass et al. developed a node-based system for assessing distance between individual polymers using Brownian dynamics.[32] Nowicki et al. simulated aggregation using a modified direct simulation method for a lattice model a colloidal-polymer system.[33] Comparison of our aggregation results against those obtained from these simulation methods is definitely a future path for exploration. Nevertheless, our work marks the beginning of a new distance-based approach for predicting aggregation of a polymer-drug system using molecular dynamics.

■ ASSOCIATED CONTENT

Ⓢ Supporting Information. Additional details for Supporting Information: Figures depicting individual coarse-grained models of 18 PGG-PTX molecules and their RMSD trajectories, unique and significant characteristic conformations, and aggregation state. Schemes displaying the procedure for determining the specific parameters of each PGG-PTX model setup. Table and sample scheme depicting results of RMSD clustering for assessing uniqueness and significance of PGG-PTX systems. Figures assessing sensitivity of PGG-PTX systems to charge state. This material is available free of charge via the Internet at http://pubs.acs.org.

■ AUTHOR INFORMATION

Corresponding Author

*E-mail: dgough@ucsd.edu.

■ ACKNOWLEDGMENT

Financial support for this work was provided by the University of California Discovery Grant bio06-10568 and Nitto Denko Technical (NDT) Corporation. L.Y. is a full-time employee of NDT and S.B.H. and D.A.G. serve as consultants for NDT on an arrangement approved by the Conflict of Interest Committee at the University of California, San Diego. L.X.P. thanks A. Ivetac for helpful technical insight and J. A. McCammon for the supercomputing resources.

■ REFERENCES

(1) Amiji, M. M. *Nanotechnology for cancer therapy*; CRC Press: Boca Raton, FL, 2007; Vol. 1, p 817.

(2) Ferrari, M. Cancer nanotechnology: opportunities and challenges. *Nat. Rev.* **2005**, *5*, 161–171.
(3) Cho, K.; Wang, X.; Nie, S.; Chen, Z.; Shin, D. M. Therapeutic nanoparticles for drug delivery in cancer. *Clin. Cancer Res.* **2008**, *14*, 1310–1316.
(4) Adiseshaiah, P. P.; Hall, J. B.; McNeil, S. E. Nanomaterial standards for efficacy and toxicity assessment. *Wiley Interdiscip. Rev.: Nanomed. Nanobiotechnol.* **2009**, *2*, 99–112.
(5) Jain, R.; Stylianopoulos, T. Delivering nanomedicine to solid tumors. *Nat. Rev. Clin. Oncol.* **2010**, *7*, 653–664.
(6) Buzea, C.; Pacheco, I. I.; Robbie, K. Nanomaterials and nanoparticles: sources and toxicity. *Biointerphases* **2007**, *2*, 17–71.
(7) Jiang, J.; Oberdorster, G.; Biswas, P. Characterization of size, surface charge, and agglomeration state of nanoparticle dispersions for toxicological studies. *J. Nanopart. Res.* **2009**, *1*, 77–89.
(8) Oberdorster, G.; Stone, V.; Donaldson, K. Toxicology of nanoparticles: a historical perspective. *Nanotoxicology* **2007**, *1*, 2–25.
(9) Moos, P. J.; Chung, K.; Woessner, D.; Honeggar, M.; Cutler, N. S.; Veranth, J. M. ZnO particular matter requires cell contact for toxicity in human colon cancer cells. *Chem. Res. Toxicol.* **2010**, *23*, 733–739.
(10) Pan, Y.; Neuss, S.; Leifert, A.; FIschler, M.; Wen, F.; Simon, U.; Schmid, G.; Brandau, W.; Jahnen-Dechent, W. Size-dependent cytotoxicity of gold nanoparticles. *Small* **2007**, *3*, 1941–1949.
(11) van Gunsteren, W. F. Molecular dynamics studies of proteins. *Curr. Opin. Struct. Biol.* **1993**, *3*, 277–281.
(12) Ng, R. *Drugs: From Discovery to Approval*; John Wiley & Sons, Inc.: Hoboken, NJ, 2004.
(13) Wang, X.; Zhao, G.; Van, S.; Yu, L. *Polymer paclitaxel conjugates and methods for treating cancer* **2009**.
(14) Vitalis, A.; Lyle, N.; Pappu, R. V. Thermodynamics of beta-sheet formation in polyglutamine. *Biophys. J.* **2009**, *97*, 303–311.
(15) Bellesia, G.; Shea, J-E Self-assembly of beta-sheet forming peptides into chiral fibrillar aggregates. *J. Chem. Phys.* **2007**, *126*, 245104–245111.
(16) Caflisch, A. Computational models for the prediction of polypeptide aggregation propensity. *Curr. Opin. Chem. Biol.* **2006**, *10*, 437–444.
(17) Pellarin, R. C.A. Interpreting the aggregation kinetics of amyloid peptides. *J. Mol. Biol.* **2006**, *360*, 882–892.
(18) Monsellier, E.; Ramazzotti, M.; Taddei, N.; Chiti, F. Aggregation propensity of the human proteome. *PLoS Comput. Biol.* **2008**, *4*, 1–9.
(19) Bratko, D.; Cellmer, T.; Prausnitz, J. M.; Blanch, H. W. Molecular simulation of protein aggregation. *Biotechnol. Bioeng.* **2007**, *96*, 1–8.
(20) Chennamsetty, N.; Voynov, V.; Kayser, V.; Helk, B; Trout, B. L. Design of therapeutic proteins with enhanced stability. *Proc. Natl. Acad. Sci. U.S.A.* **2009**, *106*, 11937–11942.
(21) de Groot, N. S., Pallares, I., Aviles, F. X., Vendrell, J., Ventura, S., Prediction of "hot spots" of aggregation in disease-linked polypeptides. *BMC Struct. Biol.* **2005**, *5*.
(22) Ma, B.; Nussinov, R. Simulations as analytical tools to understand protein aggregation and predict amyloid conformation. *Curr. Opin. Chem. Biol.* **2006**, *10*, 445–452.
(23) Nichols, G.; Byard, S.; Bloxham, M. J.; Botterill, J.; Dawson, N. J.; Dennis, A.; Diart, V.; North, N. C.; Sherwood, J. D. A review of the terms agglomerate and aggregate with a recommendation for nomenclature used in powder and particle characterization. *J. Pharm. Sci.* **2002**, *91*, 2103–2109.
(24) Peng, L. X.; Ivetac, A.; Chaudhari, A. S.; Van, S.; Zhao, G.; Yu, L.; Howell, S. B.; McCammon, J. A.; Gough, D. A. Characterization of a clinical polymer-drug conjugate using multiscale modeling. *Biopolymers* **2010**, *93*, 935–951.
(25) Marrink, S. J.; de Vries, A. H.; Mark, A. E. Coarse-grained model for semi-quantitative lipid simulations. *J. Phys. Chem. B* **2004**, *108*, 750–760.
(26) Marrink, S. J.; Rissalada, J. H.; Yefimov, S.; Tieleman, D. P.; de Vries, A. H. The MARTINI force field: coarse-grained model for biomolecular simulations. *J. Phys. Chem. B* **2007**, *111*, 7812–7824.
(27) Monticelli, L.; Kandasamy, S. K.; Periole, X.; Larson, R. G.; Tieleman, D. P.; Marrink, S. J. The MARTINI coarse-grained force field: extension to proteins. *J. Chem. Theory Comput.* **2008**, *4*, 819–834.
(28) Schlick, T. *Molecular Modeling and Simulation: An Interdisciplinary Guide*; Springer: New York, NY, 2002; Vol. 21.
(29) Peng, L. X., Das, S. K., Yu, L., Howell, S. B., Gough, D. A., Coarse-grained modeling study of nonpeptide RGD ligand density and PEG molecular weight on the conformation of poly(gamma-glutamyl-glutamate) paclitaxel conjugates. *J. Mol. Model.* **2011**.
(30) Humphrey, W.; Dalke, A.; Schulten, K. VMD - Visual Molecular Dynamics. *J. Mol. Graphics* **1996**, *14*, 33–38.
(31) MathWorks; Natick, MA, 1994−2008.
(32) Cass, M. J.; Heyes, D. M. Brownian dynamics simulations of associating diblock copolymers. *Langmuir* **2007**, *23*, 6576–6587.
(33) Nowicki, W.; Nowicka, G. Model of aggregation of colloidal fine particles in the presence of supersized polymer. *Colloid Polym. Sci.* **1995**, *273*, 298–305.